Rare Metal Materials and Engineering
Volume 52, Issue 5, May 2023
Available online at www.rmme.ac.cn

Science Press

Cite this article as: Li Hui, Wang Feng, He Wei, et al. Microstructure Characterization and Corrosion Resistance of TIG-Welded Al_3Zr/A356 Composites[J]. Rare Metal Materials and Engineering, 2023, 52(05): 1616-1623.

ARTICLE

Microstructure Characterization and Corrosion Resistance of TIG-Welded Al_3Zr/A356 Composites

Li Hui[1], Wang Feng[1], He Wei[1], Lu Shengbo[2], Sun Caizhi[1], Han Xudong[1], Shcheretskyi Volodymyr[3]

[1] School of Materials Science and Engineering, Jiangsu University of Science and Technology, Zhenjiang 212000, China; [2] Shennan Circuits Co., Ltd, Wuxi 214142, China; [3] Phisico-technological Institute of Metals and Alloys of National Academy of Science of Ukraine, Kyiv 03115, Ukraine

Abstract: The Al_3Zr/A356 aluminum matrix composites (AMCs) with 3wt% reinforcing phase were prepared by in-situ reaction method. Through X-ray diffractometer, scanning electron microscope, energy dispersive spectrometer, and microhardness tests, the microstructures and corrosion resistance of the welded joints after tungsten inert gas (TIG) welding with different welding parameters were investigated. Results show that when the welding current is 140 A, the formation of weld seam is optimal, and no welding defects, such as pores or cracks, appear. The fine Al_3Ti reinforcing particles are generated during the welding process, presenting the spherical and short rod shapes, and they are dispersed in the matrix. The hardness of the welded joint is higher than that of the base metal, and the strengthening effect of the reinforcing particles becomes obvious. With prolonging the immersion duration in 3.5wt% NaCl solution, the pitting degree of weld seam is aggravated, and the pitting mainly occurs around the grain boundaries and strengthening phases. The micro-area electrochemical experiment results show that when the welding current is 140 A, the corrosion potential fluctuation is small, the corrosion tendency is low, and the corrosion resistance is optimal.

Key words: aluminum matrix composites; TIG welding; in-situ reaction; corrosion resistance

As-cast A356 aluminum alloy is often used to replace traditional steel materials in the automotive and aerospace industries due to its lightweight, high specific strength, and good corrosion resistance[1–2]. Particle-reinforced aluminum matrix composites (AMCs) often have the defects of agglomeration and high porosity. The preparation of AMCs by the salt coating method has been widely investigated[3–7]. It is found that the Al_3Zr particles generated by salt deposition have high bonding degree and low porosity. Compared with other reinforced particles, Al_3Zr particles have good corrosion resistance and wear resistance. Thus, the combination of Al_3Zr with A356 AMCs is a worthy investigation topic. However, the weldability of particle-reinforced AMCs is inferior, and the welding of AMCs is rarely researched[8–12]. Friction stir welding is a common method for as-cast AMCs[13–18]. Tao et al[19] prepared the AA6063 AMC plates with Al_2O_3 dispersion strengthening effect by friction stir welding and post-weld heat treatment to improve the mechanical properties of the joints. In addition, the studies on as-cast A356 alloy welded by laser welding[20] and gas tungsten arc (GTA) welding[21–22] are rarely reported. Ratnakumar[23] and Arrabal[24] et al studied the corrosion behavior, partial melting zone, and heat-affected zone of A356 alloy welded by continuous and pulsed current GTA method at different temperatures. The partial melting zone of the weld is seriously corroded, and the pulsed current GTA method can reduce the corrosion degree of the partial melting zone. Tungsten inert gas (TIG) welding is suitable for most metal materials, and the appropriate parameters of TIG welding can greatly improve the welding quality.

Aluminum alloy can be easily corroded in salt water, salt spray, and acid environment, which thereby affects the service life of alloy. The reinforced phase particles with good

Received date: September 07, 2022
Foundation item: National Natural Science Foundation of China (51605206); Postgraduate Research & Practice Innovation Program of Jiangsu Province (SJCX21_1769, SJCX22_1941); Ministry of Science and Technology High-End Foreign Experts Introduction Program Project (G2022014043, G2022014134L)
Corresponding author: Li Hui, Ph. D., Professor, School of Materials Science and Engineering, Jiangsu University of Science and Technology, Zhenjiang 212000, P. R. China, E-mail: lihuiwind@163.com

corrosion resistance can improve the corrosion resistance of the matrix to a certain extent, but they can also degrade the surface integrity of composites and accelerate the corrosion process. Therefore, it is necessary to study the corrosion resistance of AMCs after TIG welding. In this research, AMCs were prepared by mixed salt method[25]. The relationship between microstructure and corrosion resistance of welded metal under different welding currents was studied, providing theoretical basis for TIG welding of Al_3Zr/A356 particle-reinforced AMCs.

1 Experiment

Al_3Zr/A356 AMCs were prepared by the in-situ synthesis method. The matrix was A356 Al alloy (Si: 0.65wt%–0.7wt%; Mg: 0.2wt% – 0.4wt%; Cu: 0.10wt%; Fe: ≤0.2wt%; Cu: ≤0.2wt%; Zn: ≤0.1wt%; Ti: ≤0.2wt%; Al: balance). K_2ZrF_6 powder was put into the drying oven, heated to 200 °C for about 2 h to remove the crystal water, and ground into powder of less than 200 μm in size. In the resistance furnace, the as-cast A356 alloy was heated to 750 °C for complete melt. Then, K_2ZrF_6 powder, as the crystal water remover, was added into the molten alloy at 750 °C. After the A356 aluminum matrix fully reacted with K_2ZrF_6 powder, AlF_3 and KF were generated and floated on the molten liquid surface during the smelting preparation due to their lightweight. After the solution was cooled, AMCs with Al_3Zr reinforcement were obtained. The chemical reaction during the preparation process[26–27] is as follows:

$$3K_2ZrF_6+13Al=3Al_3Zr+4AlF_3+6KF \quad (1)$$

The prepared AMCs with Al_3Zr reinforcement were cut into the specimens with size of 100 mm×50 mm×4 mm, and the oxidized layer was removed. The plate and Al-Ti-B welding rod were cleaned in K_2ZrF_6 aqueous solution, and the wetting angle was increased to improve the welding adhesion after complete drying. The used welding parameters are shown in Table 1.

X-ray diffractometer (XRD, Bruker D8 advance XRD) was used to analyze the phase composition of the specimens. The specimen microstructures were observed by scanning electron microscope (SEM, Carl Zeiss Merlin Compact, Germany), and the distribution, size, and morphology of the reinforced phase were observed. The microhardness at the center line of the cross section of welded joint was measured by KB Pruftechnik microhardness tester. The ballast force of the automatic microhardness tester was 0.2 kg. The micro-hardness of the base metal (BM) zone, heat affected zone (HAZ), and weld seam was tested 5 times.

The micro-area electrochemical tests were conducted by scanning Kelvin probe (SKP, PG302N, Princeton company, USA). The weld seam obtained after welding with different parameters was soaked in 3.5wt% NaCl solution for 7 and 28 d for comparative analysis. After soaking, the microstructure of the weld seam was analyzed. The corrosion morphology was observed by laser confocal microscope (LEXTOLS4000 Olympus Co., Ltd).

Table 1 TIG welding process parameters

Specimen	Welding current, I/A	Welding speed, V/mm·min^{-1}	Shielding gas flow, Q/L·min^{-1}
1	130	200	10
2	140	200	10
3	150	200	10

2 Results and Discussion

2.1 XRD analysis of weld microstructure

As shown in Fig. 1a, the diffraction peaks mainly correspond to Al, Si, Al_3Ti, and Al_3Zr phases. No other obvious diffraction peaks appear, indicating that no other substances exist in the prepared AMCs. Fig. 1b is standard PDF cards of specific phases. This is because the amount of these substances is relatively small, i.e., the diffraction peaks of these substances are very weak, or the diffraction peaks overlap with those of other substances. The phase composition of Specimen 1 and Specimen 2 is mainly Al, Si, and Al_3Ti phases, indicating that there is a fusion part in the material. The diffraction peak of Si phase appears in Al matrix, indicating that a small amount of AlSi eutectic phase is distributed in the matrix. In addition, the Al_3Zr and Al_3Ti reinforced phases also exist in the specimens. Because no fusion occurs on Specimen 3, the diffraction peaks may correspond to the covered electrode and matrix in the weld area. Thus, the main composition of Specimen 3 is Al, Si, Al_3Zr, and a small amount of Al_3Ti reinforced phase.

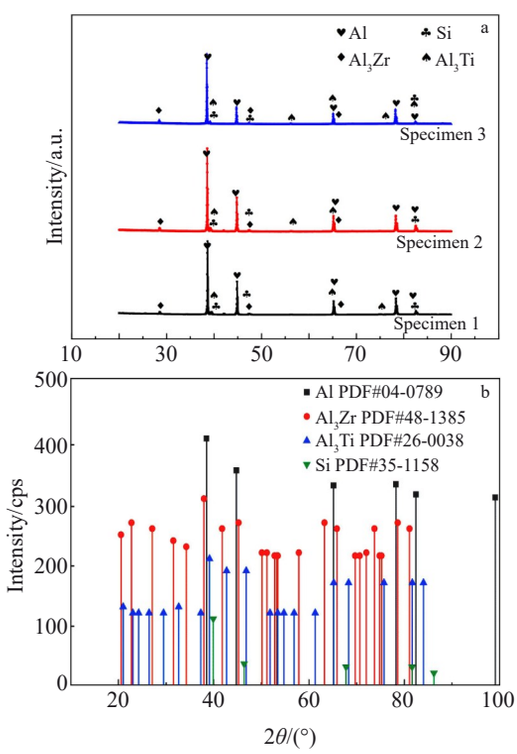

Fig.1 XRD patterns of different welding specimens (a) and standard PDF cards of specific phases (b)

2.2 Microstructure of weld seam

Fig. 2 shows SEM microstructures of fusion zone (FZ) and weld seam of welded joint of Specimen 3. It can be seen that the welding defects appear on the specimen surface, such as pores and cracks, due to the low heat input and the reinforcement phase. The fluidity of specimen is inferior, and the gas cannot overflow in time, resulting in the pores and cracks. Al_3Ti phase of long strip shape with size of 25–30 μm is densely distributed in FZ. Due to the large thermal expansion coefficient of the specimens during welding, large internal stress is generated under the local intense temperature change, and the long-reinforced phase can easily cause the stress concentration. The TiB_2 reinforcement particles can be observed in Fig. 2b due to the reaction of Ti and B elements with Al under the thermal effect of welding arc. Thus, the Al_3Ti and TiB_2 reinforced particles are formed in FZ. However, the diffraction peaks of TiB_2 particles cannot be observed by XRD, which may be due to the low TiB_2 content.

SEM microstructures of the welded joint of Specimen 2 are shown in Fig. 3. Nearly no defects appear on the weld surface. The Al_3Ti reinforcement phase is spherical and elliptical, its size is small of 20–25 μm, and it is uniformly dispersed in the weld seam. It can be clearly seen that the Al_3Ti is well bonded to the Al matrix, which plays an important role in dispersion strengthening and thereby effectively improves the strength of welded joints.

SEM microstructures of the welded joint of Specimen 1 are shown in Fig. 4. The incomplete fusion areas appear in the welding joint of Specimen 1, because the specimen has a large thermal expansion coefficient and the large internal stress is generated under local intense temperature change. In addition, the agglomeration of elongated reinforcement phases leads to the stress concentration. When the stress is greater than the

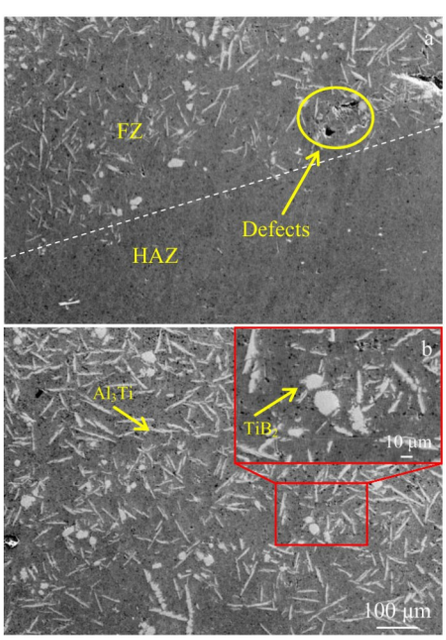

Fig.2 SEM microstructures of FZ (a) and weld seam (b) of welded joint of Specimen 3

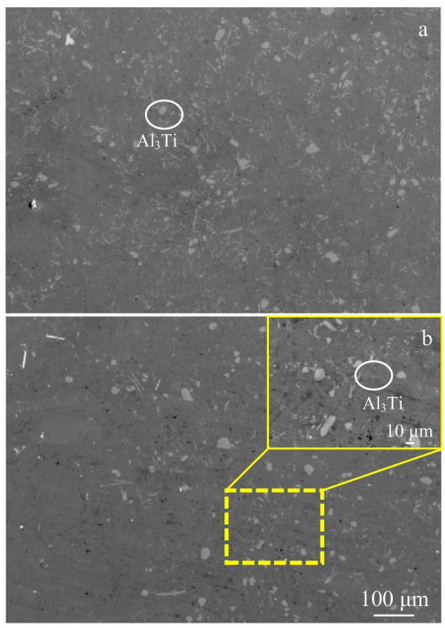

Fig.3 SEM microstructures of FZ (a) and weld seam (b) of welded joint of Specimen 2

bonding strength between the reinforcement particles and the matrix, the cracks appear at the sharp corner and expand under the force, forming a large crack. When the welding current reaches 150 A, the particle density in FZ and HAZ is much larger than that under welding current of 140 A. In FZ, Al_3Ti is mainly in the shape of long strip. Some Al_3Ti is spherical, and its agglomeration is severe.

2.3 Microhardness of weld joints

The microhardness of different welded joints is shown in Fig. 5. It can be seen that the BM microhardness of all specimens is similar to each other, and the microhardness is firstly increased and then decreased from BM to weld seam. The highest microhardness occurs in HAZ due to the effect of arc heat input, which leads to the heat treatment strengthening. However, the existence of pores and other defects in the weld seam leads to the degradation of microhardness in the weld seam. The average microhardness of different areas differs, and the Specimen 1 has the highest microhardness because of its high content of Al_3Ti reinforcement phase in the welded joint. The highest microhardness of BM, HAZ, and weld seam is 507.05, 603.29, and 542.82 MPa, respectively.

2.4 Corrosion resistance of welded joints

SEM microstructures of different welded joints after immersion in 3.5wt% NaCl solution for different durations are shown in Fig. 6. It can be seen that after immersion for 7 d, the weld structure is obviously corroded, and the corrosion products and pits are generated. As shown in Fig. 6a–6c, the oxygen content of Specimen 1, Specimen 2, and Specimen 3 is 61.86at%, 55.72at%, and 59.62at%, respectively. Because of the oxide film, the welded joint is protected from the corrosive medium. Thus, the corrosion of the welded structure is inhibited. As shown in Fig. 6a, 6c, and 6e, the grain

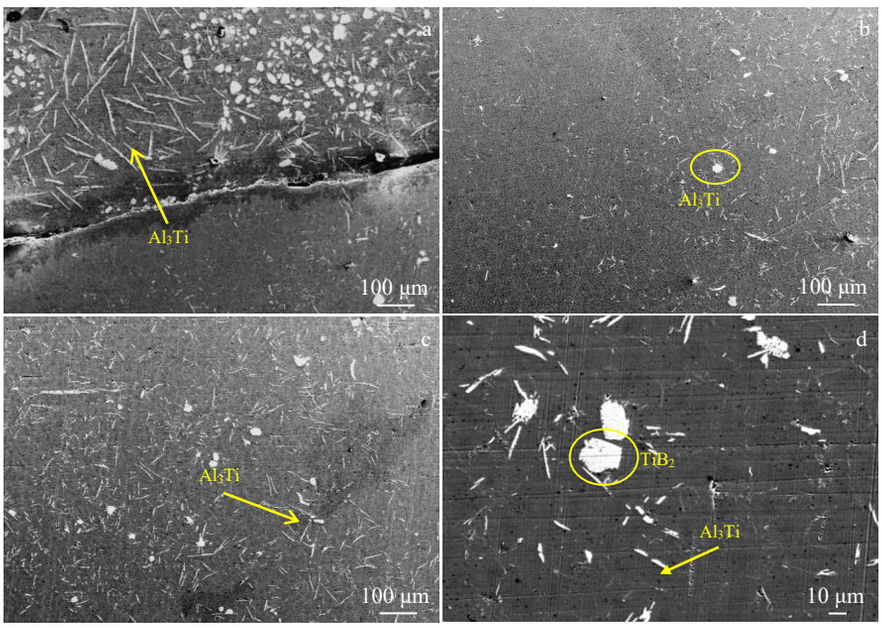

Fig.4 SEM microstructures of FZ (a–b), weld seam (c), and HAZ (d) of welded joint of Specimen 1

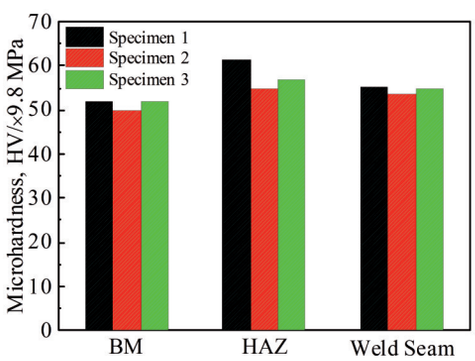

Fig.5 Microhardness of BM, HAZ, and weld seam of different welded joints

boundaries of AMCs are preferentially corroded, and multiple cracks occur at the grain boundaries. Combined with XRD results, it is found that there are a large number of AlSi compounds, and the grain boundaries are mainly composed of AlSi compounds and Si. The electrochemical inhomogeneity of the matrix leads to the fast corrosion rate at the grain boundary and the slow corrosion rate of the matrix, which promotes the formation of intergranular corrosion. With prolonging the corrosion duration to 28 d, the oxygen content of Specimen 1, Specimen 2, and Specimen 3 is 64.38at%, 62.81at%, and 63.92at%, respectively, suggesting a decreased corrosion rate. As shown in Fig. 6b, 6d, and 6f, after immersion for 28 d, the corrosion pits on welded surface are increased, and macro-cracks appear. The reinforcement phase can hardly be corroded. Thus, the corrosion resistance of AMCs with reinforcement phase is enhanced, as well as that of the welded structure.

In the formation process of aluminum oxide film in the low activity region, the oxide film can passivate the composite material, as follows:

$$Al-3e^{-}=Al^{3+} \quad (2)$$

$$Al^{3+}+3OH^{-}\rightarrow Al(OH)_3 \quad (3)$$

$$2Al(OH)_3\rightarrow Al_2O_3+3H_2O \quad (4)$$

In the high activity region, a large amount of Cl^{-} accumulates in the oxide film. When the concentration reaches a certain level, the anodic dissolution reaction[28] occurs, as follows:

$$Al-3e^{-}=Al^{3+} \quad (5)$$

$$Al^{3+}+3H_2O\rightarrow Al(OH)_3+3H^{+} \quad (6)$$

$$Al^{3+}+4Cl^{-}\rightarrow AlCl_4^{-} \quad (7)$$

$$AlCl_4^{-}+3H_2O\rightarrow Al(OH)_3+3H^{+}+4Cl^{-} \quad (8)$$

With the acceleration of ionization on the bare Al surface, the concentration of Al^{3+} in the etched hole is increased and the Cl^{-} ions migrate to the hole, which leads to the increase in Cl^{-} and H^{+} concentrations in the etch holes. Therefore, the solution inside the etch hole is acid, and the Cl^{-} and H^{+} ions produced by hydrolysis result in the continuous dissolution of aluminum in the etch hole, and the corrosion product $Al(OH)_3$ is generated. With the corrosion and accumulation proceeding, the pitting corrosion expands rapidly[29].

When the welding current is 130 A (Specimen 1), the corrosion of the welded joint is more serious, because the heat input is relatively low, which results in more corrosion pits. When the welding current is 140 A (Specimen 2), the irregular cracks are generated around the reinforcement phase and the crystal grains, and small part of the oxide film falls off. The reinforcement phase is distributed uniformly in the weld seam, resulting in the good corrosion resistance of welded joint. When the welding current is 150 A, the heat input is the highest, and more AlSi compound is generated, which forms the galvanic couple with the matrix and thereby leads to the

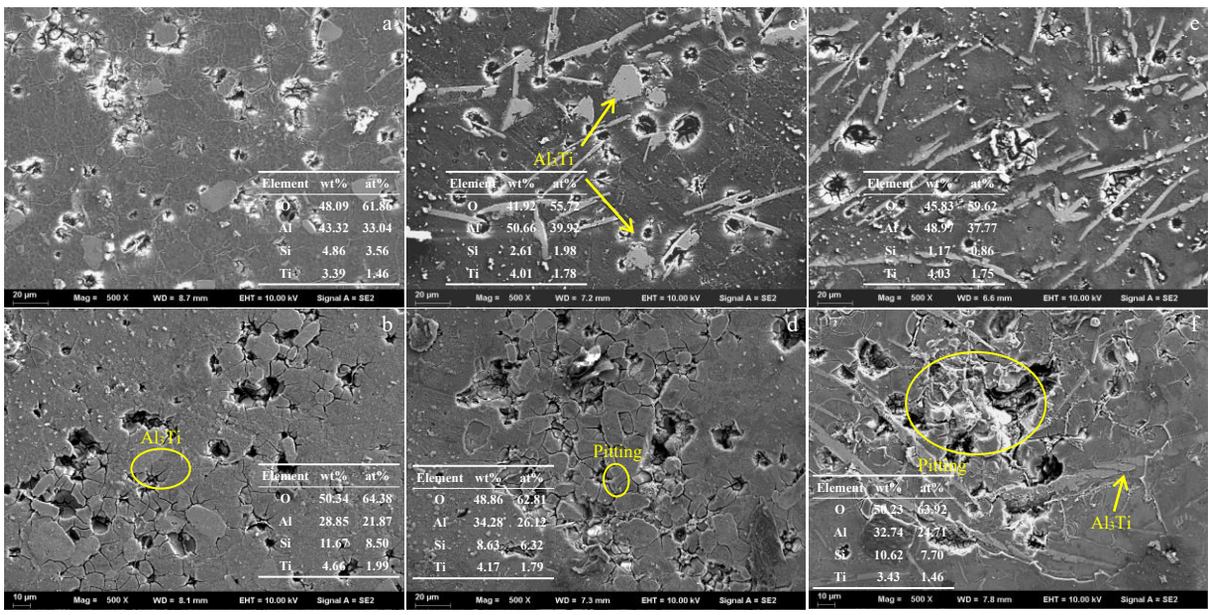

Fig.6 SEM microstructures and EDS analysis results of Specimen 1 (a–b), Specimen 2 (c–d), and Specimen 3 (d–f) after immersion in 3.5wt% NaCl solution for 7 d (a, c, e) and 28 d (b, d, f)

intergranular corrosion. In this case, the reinforcement phase agglomerates severely, and many corrosion pits appear at the interface between the reinforcement phase and the matrix. After immersion for 28 d, the interface between the matrix and the reinforcement phase cracks, and the reinforcement phase tends to fall off, leading to the severe corrosion.

Fig. 7 shows XRD patterns of different welded joints after

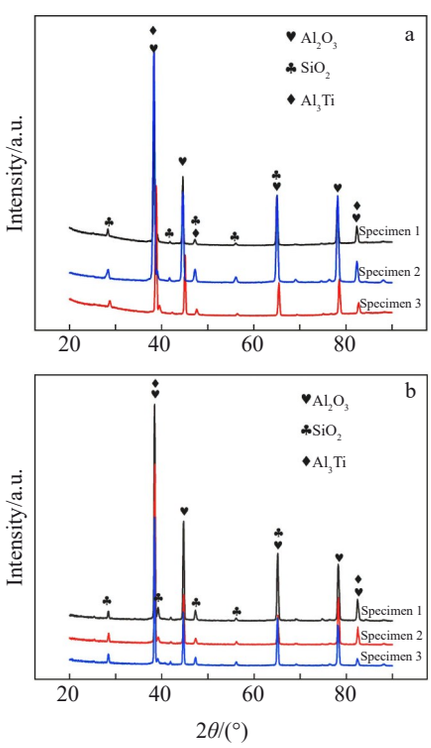

Fig.7 XRD patterns of different welded joints after immersion in 3.5wt% NaCl solution for 7 d (a) and 28 d (b)

immersion in 3.5wt% NaCl solution for 7 and 28 d. It can be seen that after corrosive immersion for 7 d, a large number of oxides (Al_2O_3 and SiO_2) are produced, the surface of welded joint is oxidized, and the oxide film is formed, which can inhibit the further corrosion. As shown in Fig. 7a, the diffraction peak of Specimen 3 is slightly shifted to the right side, compared with that in Fig. 1a. This is because with increasing the heat input, the volume of the reinforcement particles becomes larger, and the doping phenomenon of the matrix becomes serious. According to Fig.7b, more oxides can be observed, but the Al_3Ti reinforcement phase cannot be oxidized, indicating its good corrosion resistance.

Fig. 8 shows the laser confocal morphologies of Specimen 1, Specimen 2, and Specimen 3 after immersion in 3.5wt% NaCl solution for 28 d. Fig.9 shows the average corrosion pit depths of different welded joints after immersion in 3.5wt% NaCl solution for 28 d. When the welding current is 130, 140, and 150 A, the corrosion pit depth is 24.360, 13.496, and 14.738 μm, respectively. It is revealed that when the welding current is 130 A, there are many corrosion pits and their corrosion pit depth is the largest, resulting in the easy connection among the corrosion pits mainly around the reinforcement phase. When the welding current is 140 and 150 A, the corrosion pit depths are similar. When the welding current is 140 A, the minimum depth of corrosion pit is obtained as 13.496 μm, and more corrosion pits appear, because the Al_3Ti reinforcement phase is dispersed in the matrix and can easily form the galvanic couple. When the welding current is 150 A, many defects occur and some corrosion pits are deep, suggesting the inferior corrosion resistance of welded joint.

SKP images from the weld center to the BM side are shown in Fig. 10, and the potential difference between the welded

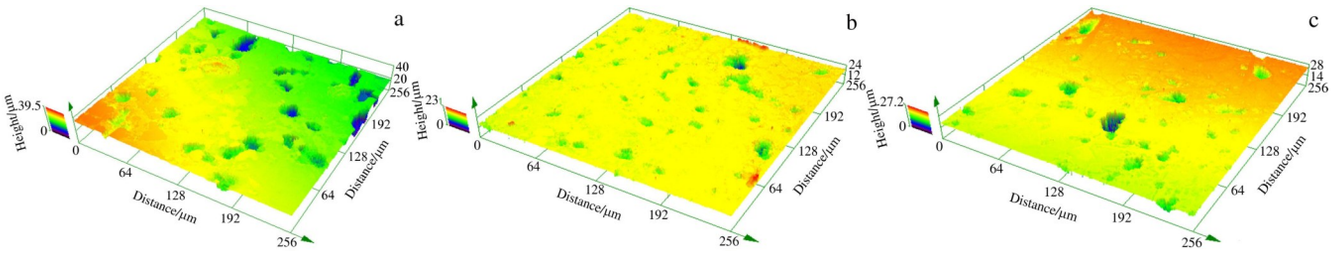

Fig.8 Laser confocal morphologies of Specimen 1 (a), Specimen 2 (b), and Specimen 3 (c) after immersion in 3.5wt% NaCl solution for 28 d

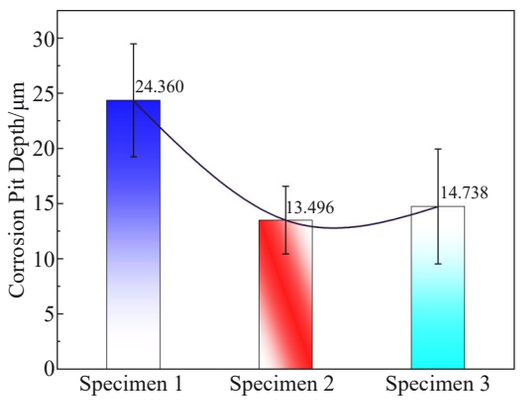

Fig.9 Corrosion pit depths of different welded joints after immersion in 3.5wt% NaCl solution for 28 d

area and BM is analyzed[30–34]. As shown in Fig. 10a and 10b, when the welding current is 130 A, many defects appear on the welded surface due to the low heat input, and the electric potential distribution is uneven. The potential decreases firstly and then increases. The potential of HAZ varies from −1082 mV to −949 mV, while the central potential of weld seam varies from −712 mV to −634 mV. The potential of HAZ is obviously lower than that of weld seam, indicating the higher corrosion tendency of HAZ. The potential fluctuation of the weld seam is large and its corrosion resistance is inferior. When the welding current is 140 A, the potential fluctuation of the welded joint is increased with varying from BM to weld seam. This is because the Al_3Ti reinforcement phase is generated, which results in large potential difference and better corrosion resistance. When the welding current is 150 A, small

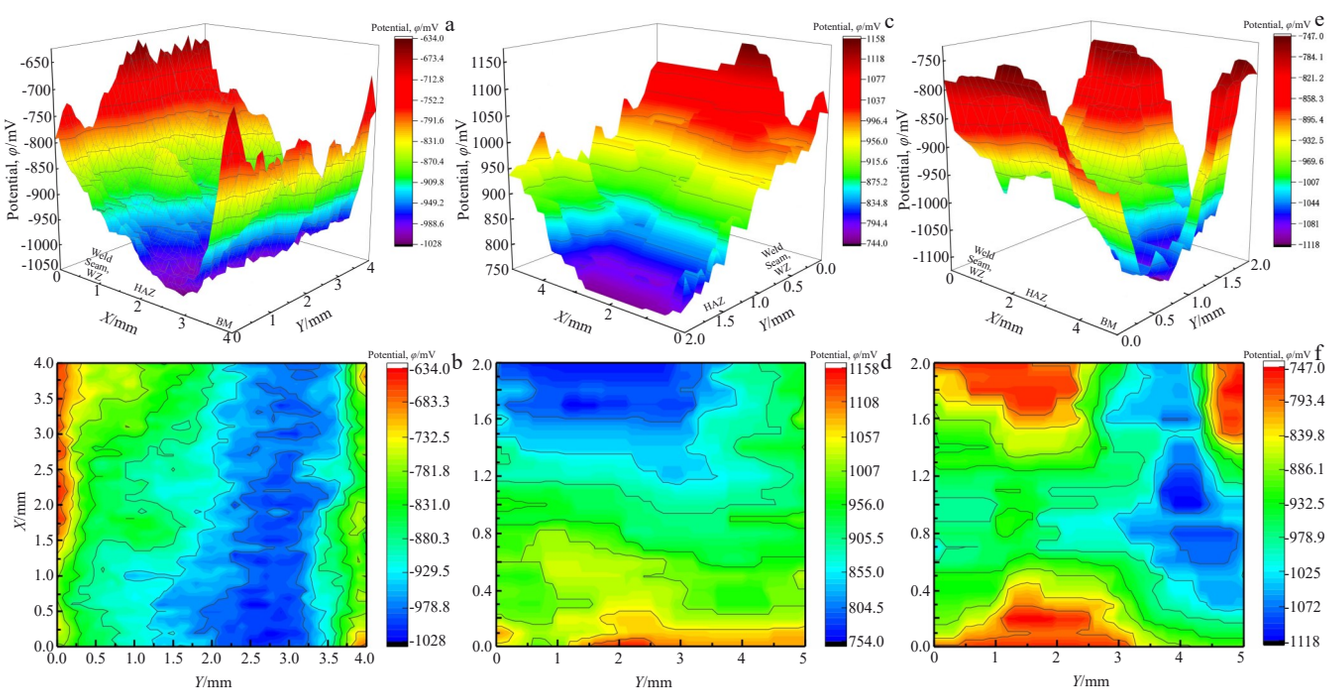

Fig.10 SKP images (a, c, e) and contour maps (b, d, f) of Specimen 1 (a–b), Specimen 2 (c–d), and Specimen 3 (e–f)

part of the potential fluctuates greatly. This is because there are some unfused areas in the welded joints, which results in many defects, serious agglomeration of reinforcement phases, and high corrosion tendency. The large potential fluctuation leads to the inferior corrosion resistance of the welded joint.

3 Conclusions

1) The Al_3Zr/A356 aluminum matrix composites (AMCs)

prepared by tungsten inert gas (TIG) welding at 750 °C with welding current of 130 A have less fusion zone and more welding defects due to the insufficient heat input. However, when the current is 150 A, an oxide film is formed, which causes the even worse fusion state and more cracks. The shape of the Al_3Ti reinforcement phase is changed with increasing the heat input. When the heat input is too large, the reinforcement phase grows quickly and becomes thicker as a long strip. When the welding current is 140 A, the formation of weld seam is optimal, and the grains of fusion zone are refined. The Al_3Ti reinforcement particles formed and dispersed in the weld seam are fine (size of about 15 μm) and mainly show the spherical shape. Some reinforcement phases show the strip shape, and they have high microhardness.

2) The Al_3Ti reinforcement phase cannot be corroded, indicating the good corrosion resistance. When the welding current is 130 A, the heat input is small, and the defects such as pores and cracks may easily occur. The potential distribution of the welded joint is quite uneven, suggesting the inferior corrosion resistance and the appearance of deep corrosion holes. When the welding current is 150 A, the reinforcement phase is coarse and it agglomerates severely, which is prone to galvanic corrosion at the interface between the reinforcement phase and the substrate, thereby leading to serious corrosion damage and degraded corrosion resistance. When the welding current is 140 A, the pitting corrosion occurs around the reinforcement phase. The corrosion pit depth is the minimum of 13.496 μm. The dispersive distribution of Al_3Ti reinforcement phase contributes to the excellent corrosion resistance of welded joint.

References

1 Kumar T S, Balasubramanian V, Sanavullah M Y. *Materials & Design*[J], 2007, 28(7): 2080

2 Babu S, Kumar T S, Balasubramanian V. *Transactions of Nonferrous Metals Society of China*[J], 2008, 18(5): 1028

3 Zhang S L, Zhao Y T, Chen G *et al*. *Journal of Alloys & Compounds*[J], 2007, 429(1–2): 198

4 Zhao Y T, Zhang S L, Chen G *et al*. *Materials Science & Engineering A*[J], 2008, 487(1–2): 1

5 Liu L, Li W W, Tang Y P *et al*. *Wear*[J], 2009, 266(7 – 8): 733

6 Jiao L, Zhao Y T, Wu Y *et al*. *Rare Metal Materials and Engineering*[J], 2014, 43(1): 6

7 Zhao Y T, Zhang S L, Chen G *et al*. *Materials Science & Engineering A*[J], 2007, 457(1–2): 156

8 Ghosh M, Husain M M, Kumar K *et al*. *Journal of Materials Engineering & Performance*[J], 2013, 22(12): 3890

9 Lee W B, Yeon Y M, Jung S B. *Scripta Materialia*[J], 2003, 49(5): 423

10 Li Hui, Jiao Lei, Lu Pengcheng *et al*. *Rare Metal Materials and Engineering*[J], 2018, 47(2): 588 (in Chinese)

11 Jiao Lei, Zhao Yutao, Yin Houshang *et al*. *Rare Metal Materials and Engineering*[J], 2016, 45(9): 2391 (in Chinese)

12 Li Hui, Jiao Lei, Mei Yunzhu *et al*. *Rare Metal Materials and Engineering*[J], 2017, 46(10): 3017 (in Chinese)

13 Lee W B, Yeon Y M, Jung S B. *Materials Science & Engineering A*[J], 2003, 355(1–2): 154

14 Amirizad M, Kokabi A H, Gharacheh M A. *Materials Letters*[J], 2006, 60(4): 565

15 Ghosh M, Kumar K, Kailas S V *et al*. *Materials & Design*[J], 2010, 31(6): 3033

16 Rajakumar S, Balasubramanian V. *Materials & Design*[J], 2010, 31(9): 4567

17 Hassan A S, Mahmoud T S, Mahmoud F H *et al*. *Science and Technology of Welding & Joining*[J], 2013, 15(5): 414

18 Takhti S, Reihanian M, Ashrafi A. *Transactions of Nonferrous Metals Society of China*[J], 2015, 25(7): 2137

19 Tao X C, Chang Y Q, Guo Y H *et al*. *Materials Science & Engineering A*[J], 2018, 725: 19

20 Akhter R, Ivanchev L Burger H P. *Materials Science & Engineering A*[J], 2007, 447(1–2): 192

21 Wang Y P, Qi B J, Cong B Q *et al*. *Journal of Manufacturing Processes*[J], 2018, 34(A): 179

22 Hwang L R, Gung C H, Shih T S. *Journal of Materials Processing Technology*[J], 2001, 116(2–3): 101

23 Ratnakumar K, Rao K S. *Transactions of the Indian Institute of Metals*[J], 2008, 61(4): 283

24 Arrabal R, Mingo B, Pardo A *et al*. *Corrosion Science*[J], 2013, 73(8): 342

25 Li H, Qiao Y P, Lu S B *et al*. *Journal of Materials Engineering and Performance*[J], 2022, 31: 5221

26 Zhang S L *et al*. *Journal of Materials Processing Technology*[J], 2007, 184(1–3): 201

27 Jiao L, Yang Y G, Li H *et al*. *Materials Research Express*[J], 2018, 5(5): 56 515

28 Ismael M K. *Eng & Tech Journal*[J], 2011, 29(8): 1482

29 Song F X, Zhang X M, Liu S D *et al*. *Transactions of Nonferrous Metals Society of China*[J], 2013, 9(23): 2483

30 Joensson M, Thierry D, Lebozec N. *Corrosion Science*[J], 2006, 48(5): 1193

31 Gerlich A, Yamamoto M, North T H. *Metallurgical and Materials Transactions A*[J], 2007, 38(6): 1291

32 Stratmann M, Leng A, Furbeth W *et al*. *Progress in Organic Coatings*[J], 1996, 27(1–4): 261

33 Egorkin V S, Medvedev I M, Sinebryukhov S L *et al*. *Materials*[J], 2020, 13(12): 2739

34 Kandasamy S, Rathinasamy P, Nagarajan N *et al*. *Anti-Corrosion Methods and Materials*[J], 2020, 67(4): 345

TIG焊Al_3Zr/A356复合材料的显微组织特征和耐腐蚀性能

李　惠[1]，王　峰[1]，何　炜[1]，陆圣波[2]，孙才智[1]，韩旭东[1]，沃洛德梅尔·谢列茨基[3]

(1. 江苏科技大学 材料科学与工程学院，江苏 镇江 212000)

(2. 深南电路股份有限公司，江苏 无锡 214142)

(3. 乌克兰国家科学院金属和合金物理技术研究所，乌克兰 基辅 03115)

摘　要：通过原位反应法制备了增强相含量为3%（质量分数，下同）的Al_3Zr/A356铝基复合材料（AMCs）。通过X射线衍射仪、扫描电子显微镜、能谱仪和显微硬度测试，研究了不同钨极氩弧（TIG）焊焊接参数下焊接接头的显微组织和耐腐蚀性能。结果表明，当焊接电流为140 A时，焊缝成形最好，没有气孔或裂纹等焊接缺陷。焊接过程中生成细小的Al_3Ti增强颗粒，呈球形和短棒状，并分散在基体中。焊接接头的硬度高于基体金属的硬度，增强颗粒的强化效果明显。随着在3.5% NaCl溶液中的浸泡时间延长，焊缝的点蚀程度增加，且大多发生在晶界和强化相周围。微区电化学实验结果表明，当焊接电流为140 A时，腐蚀电位波动小，腐蚀倾向低，耐腐蚀性能最好。

关键词：铝基复合材料；TIG焊；原位反应；耐腐蚀性能

作者简介：李　惠，女，1979年生，博士，教授，江苏科技大学材料科学与工程学院，江苏 镇江 212000，E-mail：lihuiwind@163.com